IJRCS
International Journal of Robotics and Control Systems
Vol. 3, No. 2, 2023, pp. 315-329
ISSN 2775-2658
http://pubs2.ascee.org/index.php/ijrcs

Dynamic Model of a Robotic Manipulator with One Degree of Freedom with Friction Component

Jose A. G. Luz Junior [a,1], Jose M. Balthazar [a,2], Mauricio A. Ribeiro [b,3], Frederic C. Janzen [b,4], Angelo M. Tusset [b,5,*]

[a] Department of Electrical Engineering, São Paulo State University, Faculty of Mechanical Engineering of Bauru, Av. Eng. Luiz Edmundo C. Coube 14-01 - Vargem Limpa, Bauru 17033-360, SP, Brazil
[b] Federal University of Technology – Paraná – Doutor Washington Subtil Chueire St., 330, Ponta Grossa – Paraná – 84017-220, Brazil
[1] jose.adg@hotmail.com; [2] jmbaltha@gmail.com; [3] mau.ap.ribeiro@gmail.com; [4] fcjanzen@utfpr.edu.br; [5] tusset@utfpr.edu.br
* Corresponding Author

ARTICLE INFO

Article history
Received April 01, 2023
Revised April 28, 2023
Accepted May 04, 2023

Keywords
Robotic Dynamics;
Friction;
LuGre;
Parameter Identification

ABSTRACT

This research aims to develop a dynamic model of a robotic manipulator with one degree of freedom by incorporating the LuGre friction model. The study combines a mathematical model with experimental data analysis, using the Stribeck curve and Non-linear Least Square method for Parameter Identification. The purpose of the study is to improve the accuracy of the model and enhance the performance of robotic manipulators. The LuGre model is chosen for its ability to capture the nonlinear behavior of friction, which is a significant source of error in robot control systems. The effectiveness of the proposed representation is evaluated by comparing the simulation results of the dynamic model with experimental data obtained from a prototype. The results indicate that the model accurately captures the nonlinear behavior of friction, and the proposed approach can be used to develop more accurate models for control purposes.

1. Introduction

Robotic manipulators have numerous applications, both in industry and in areas outside the industrial environment, such as in medical applications. Because they are similar to the human arm, they can be used to replace humans in risky activities, such as handling radioactive materials or handling materials with the risk of biological contamination, among many others [1]-[3]. The field of study of applications and improvements of robotic manipulators has shown promise in recent years, leading researchers from academia and industry to develop applied research on robotic manipulators, contributing to scientific advances and meeting industrial needs [4]-[6].

Among the developed research, we can mention the dynamics and control of manipulators, which are being developed by several researchers. In the literature, several approaches applied to the control of robotic systems are presented. In [7], a combination of Slider Mode Control (SMC) and PID control is presented. In [8], the use of optimal control is presented, while in [9], PID control is used, and Model Predictive Control (MPC) in [10]. With regard to non-linear controls, those reported in

[11]-[13] can be considered. The work [14] presents a controller based on a Fuzzy-PID control and self-tuning SMC, including in the investigation a Time Delay Estimation (TDE–Time Delay Estimation). The works of [15] and [16] consider the use of adaptive control for robotic manipulators. Numerical simulations presented in both works demonstrate that the controllers performed well, with the advantages of presenting excellent tracking with high accuracy and robustness. In work [17], a predictive control model (MPC–Model Predictive Control) is presented for a two-link planar robotic arm. In [18]-[21], the non-linear controller SDRE (State Dependent Riccati Equation) is considered to control a robotic manipulator with two degrees of freedom and with flexible joints. While in [22]-[23], the SDRE control is designed for a robotic manipulator with 2 degrees of freedom and a non-ideal excitation source. Positioning control of a robotic manipulator subjected to vibrations originating from a non-ideal excitation source is also presented in [24], [25] being combined PID-LQR controls and feedforward control. In [26], a Complex Fractional Order (CFO) Linear Quadratic Integral Regulator (LQIR) is proposed. Experimental results demonstrated the efficiency of the proposed control (CFO-LQIR) in comparison with its integer and fractional order equivalents. In [27], an Integral Slider Mode Control (ISMC) is proposed for a robotic arm with five Degrees of Freedom (DOF). In the control design, the authors considered friction compensation by the LuGre model. Numerical simulations and experimental results are presented to demonstrate the efficiency of the proposed control in trajectory tracking. A control algorithm that combines Fast integral Sliding-mode Control (FIT-SMC) with a Robust Exact Differentiator Observer (RED) and Feedforward Neural Network-based Estimator (FFNN) is presented in [28]. In [29], the control techniques of the Linear Quadratic Regulator (LQR) and Integral Proportional (PI) and Integral (I) are applied and compared for the position control of a serial robotic manipulator with 4 Degrees of Freedom (DOF). In [30] considers a non-singular terminal slip-mode controller using an optimization technique using a hybrid metaheuristic method for a robotic manipulator with three degrees of freedom.

Considering the control problem for tracking movements, one of the main problems that impede fast tracking behavior of robotic manipulators is friction [31]-[33]. Non-linear friction often disturbs a control system and can even make it unstable [34], [35]. Consequently, friction is an intrinsically non-linear occurrence that is difficult to predict [36]. Estimation of joint friction by the de LuGre model has proven to be an efficient way to include the influence of friction in the dynamics and position control of the links in robotic manipulators [37], [38]. In [37], an integral sliding mode control (ISMC) is proposed for a robotic arm with five degrees of freedom (DOF). The proposed control considered friction compensation by the LuGre model. The friction compensation of the manipulator's joints by the LuGre model is also considered in [38]. Being considered a robotic arm with five degrees of freedom (DOF), controlled by fast integral sliding mode (FIT-SMC), with a robust exact differentiator (RED) observer and an estimator based on a feedforward neural network (FFNN).

In this scenario, the modern control of robotic systems has advanced more and more into the direction of undemanding how the various physical phenomena like friction, clearance and wear involved in the movement of the links influence the efficiency of the control. That is, in addition to an effective control system that seeks to guide the robot’s links, the modern approach seeks to understand how they influence the feedback and how introducing them into the robot model makes the control more effective. Although it is possible to design a control system that ignores or indirectly includes these phenomena, the effectiveness is always committed to a restricted application window since disturbance can arise from them and the control system is not designed to deal with them.

Friction, Dead Zone and Clearance are examples of that phenomenon that directly influence the control system e has been more and more subject of studies [39]. Keeping in mind that it is impracticable to use a mathematical model that covers all the possible disturbances, it is in the engineer's hands the judgment each one is more relevant and what is the best way to include them in the final model.

In robotics, friction is a dissipative force that acts against movement imposed by the actuators when two surfaces are in contact and when one of them is moving. Due to that is a force dependent on components like the geometry of the surfaces, type and temperature of the materials, velocity between them and a number of other factors a purely mathematical model very hard to find in [40] points out as the best alternative to a good friction model is the combination of experiment and mathematical model. The mathematical model is responsible for representing the physical phenomena and the experiment in formatting so that it represents the studied system well.

Considering the problem presented, this work proposes a friction component for the first link of the robotic manipulator with three degrees of freedom with DC motor as actuators, as shown in the 3D Project in Fig. 1(a) and the prototype in Fig. 1(b).

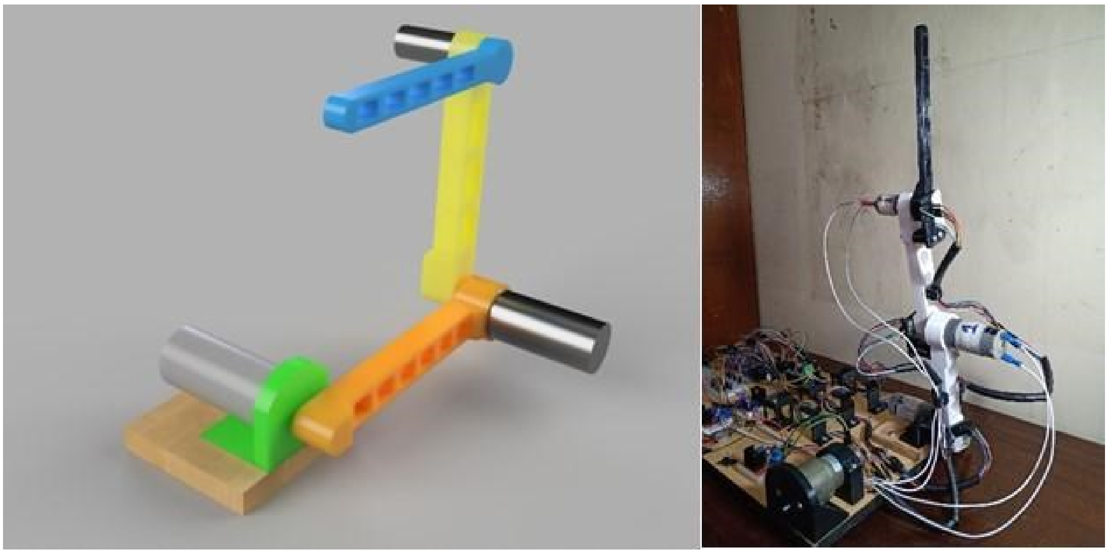

(a) (b)

Fig. 1.(a) Robotic Manipulator Project in Fusion 360 Software (b) Robotic Manipulator Prototype with 3 Degrees of Freedom

This research seeks to contribute to the advancement of the representation of mathematical models applied in robotic systems through the presentation and proposition of a method for defining the friction parameters of the LuGre model. By obtaining experimental data from a manipulator prototype, the results obtained make it possible to determine a mathematical model of the friction of the LuGre model, thus making it possible to analyze its internal phenomena, such as the stick and slip motion and the pre-sliding displacement, behavior arising from friction.

The paper is organized as follows: The introduction presents some of the most recent contributions to the research topic and the contribution of the present work to the body of knowledge. In the Method section, we present the mathematical model of the robot dynamics and LuGre friction, the form of parameter acquisition and experimental configuration. The Results and Discussions section presents the experimental results. Finally, in the Conclusion, we present the conclusions of the results presented in the paper body.

2. Method

2.1. Robot Dynamics and LuGre Friction Model

The robotic system description can be done using several methods, from analytical to specific methods, such as Denavit-Hartenberg and Kane's Formulations. Regardless of the method, describing the dynamics in a matrix form is fundamental in models involving friction since they relate the forces with positions and velocities, allowing us to isolate the terms according to their influence and physical meaning. Equation (1) shows the most common dynamic model for a robotic system:

$$M(\theta)\ddot{\theta} + C(\theta,\dot{\theta})\dot{\theta} + G(\theta) + \tau_f = \tau \tag{1}$$

Where τ_f is the robot joint friction torque, $M(\theta)$ is the inertia matrix, $C(\theta,\dot{\theta})$ is the coupling and centrifugal matrix, $G(\theta)$ is the gravitational matrix, and τ is the control input torque.

The system used in this work was part of the prototype presented in Fig. 1, as only the first link of the system was used, turning the robot into a manipulator with one degree of freedom. The manipulator dynamics can be obtained using the Denavit-Hartenberg kinematics method, where the derivative of the position matrix A_i shown in (6) compose calculation of the Euler-Lagrange dynamics [39], [40]. For a robot with $i = 1$ degrees of freedom, the dynamics is given by:

$$\tau_1 = D_{11}\ddot{\theta}_1 + D_{111}\dot{\theta}_1^2 + D_1 \tag{2}$$

where D_{11}, D_{111} and D_1 are components given by:

$$D_{11} = Trace(U_{11}J_1U_{11}^T) \tag{3}$$

$$D_{111} = Trace(U_{111}J_1U_{11}^T) \tag{4}$$

$$D_1 = -m_1g^TU_{11}\bar{r}_1 \tag{5}$$

$$A_1 = \begin{bmatrix} C\theta_1 & -S\theta_1 & 0 & a_1C\theta_1 \\ S\theta_1 & C\theta_1 & 0 & a_1S\theta_1 \\ 0 & 0 & 1 & 0 \\ 0 & 0 & 0 & 1 \end{bmatrix} \tag{6}$$

The components U_{11} and U_{111} are the derivatives of the matrices A_i in terms of θ_1 such as $U_{11} = \frac{\partial A_1}{\partial \theta_1}$ and $U_{111} = \frac{\partial(\partial A_1}{\partial \theta_1)}/\partial\theta_1$, J_1 is the link $i = 1$ inertia matrix, g is the gravitational matrix and $\bar{r}_1$ is a vector representing a point in the link $i = 1$ using the coordinate system used to represent the robot. Written the dynamic equation in matrix form as shown in (1), the model with friction component is given by:

$$[0.3l_1^2m_1 - a_1l_1m_1 + a_1^2m_1][\ddot{\theta}_1] + [9.8m_1l_1a_1\cos(\theta_1) - 4.9m_1l_1\cos(\theta_1)] + \tau_f = \tau_1 \tag{7}$$

The definition of the friction component τ_f involves the theoretical comprehension of the numerous friction models and how each one has a better fit with the system in such a way that the model is capable of describing the most important phenomenal present on the robot.

The LuGre friction model is one of the most well-established models in robotics due to the fact that it is capable of representing the most important components and has a viable experimental approach [43]-[48]. LuGre is a dynamic friction model presented by [43] as a derivation from the Dahl Model [49] and the Bristle Model from Haessig and Friedland [47]. From the Bristle Model from Haessig and Friedland [50], the LuGre model describes the relationship between two surfaces in contact as one composed of rigid bristles and the other one with massless bristles. The contact and the input force on the surfaces deform the bristles in a spring-analogous way, and the friction force is given by the sum of all spring forces, as shown in Fig. 2.

The LuGre Model by [43] describes the average bristles deformation by the variable z, as shown in Fig. 2, and the friction force is given by three equations as

$$F = \sigma_0 z + \sigma_1(\frac{dz}{dt}) + \sigma_2\dot{\theta} \tag{8}$$

$$\frac{dz}{dt} = \dot{\theta} - \frac{|\dot{\theta}|}{g(\dot{\theta})}z \tag{9}$$

$$\sigma_0 g(\dot{\theta}) = F_C + (F_S - F_C)e^{-\left|\frac{\dot{\theta}}{\dot{\theta}_S}\right|^2} \tag{10}$$

where z is the average amount of deformation of the bristles, $g(\dot{\theta})$ the Stribeck Effect, F_C the coulomb friction, F_S the maximum static friction force, $\dot{\theta}_S$ the Stribeck velocity, σ_0 the stiffness coefficient, σ_1 the setae damping coefficient and σ_2 the coefficient of viscous friction.

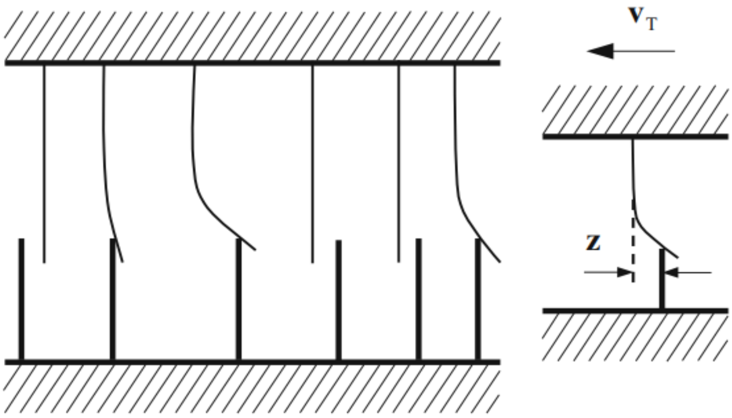

Fig. 2. Bristles Deformation in the LuGre Model

From the system shown in (8) to (10) is possible to see that besides the components of friction torque and velocity, $F(\dot{\theta})$ and $\dot{\theta}$, there are six parameters, F_c, F_s, $\dot{\theta}_S$, σ_2, σ_0 and σ_1, that describes the friction model. These six parameters can be obtained through a comparative analysis between the mathematical model and experimental data.

2.2. Parameters Acquisition and Experimental Setup

As pointed out by [43] and [45], the component in z (8) to (10) is not measurable experimentally, so the friction model and parameter acquisition must be made indirectly. The six parameters that need to be found presented in those equations can be divided into two groups, those called Static Parameter, F_c, F_s, $\dot{\theta}_S$ and σ_2, and the Dynamic Parameters, σ_0 and σ_1.

The division into two groups comes from the theoretical interpretation of what is described by them, and, in a general sense, the dynamic parameters are linked to the moment immediately before the movement to a defined point of low velocity and the static parameters beyond that defined point and the steady-state [51]. In addition to the theoretical origin, this division aims to guide the experimental procedure since there is a big difference in how the experimental data needs to be obtained for each one of them.

This distinction will be discussed in its own section, but there is common ground from both, find the relationship between the links friction force and velocity. The velocity data is measured by position differentiation, but the friction data requires some additional explanations. As shown by the (7) to (10), the friction force is dependent on movement. Therefore, there are two forces that can cause motion in the robotic manipulators, the actuators and gravity.

Based on the system described in (1), beyond the friction and gravity terms, the robotic manipulators have three more components, the inertia matrix $M(\theta)$, the Coriolis and centrifugal matrix $C(\theta, \dot{\theta})$ and the input torque τ. As shown by [44], the Coriolis and centrifugal component $C(\theta, \dot{\theta})$ can be eliminated by analyzing one isolated joint as shown by [52], or by keeping the joint locked and moving only the studies joint, as discussed by [53]. The inertia matrix $M(\theta)$ is null when the link velocity is constant, $\dot{\theta}$ = constant and $\ddot{\theta} = 0$, leading to a simplification in (1) as:

$$\tau_f + G(\theta) = \tau \tag{11}$$

This leads to two approaches to finding the friction torque τ_f, isolating the link making $G(\theta)$ null or using numerical simulation to find the values for $G(\theta)$. It leads to the input torque τ being equal to the friction torque τ_f when one of the presented procedures is followed.

Since most manipulators do not have force sensors in each link, the friction forces can be measured in an indirect form through the actuator current. In [53] shows the process known as Virtual Torque Sensor and how it can be used for this acquisition process.

$$\tau_j = K_{t,j} i_j \tag{12}$$

where i_j is the current for the j DC motor and $K_{t,j}$ is the torque constant for the j DC motor.

With the friction torque and velocity data, it is possible to build the Stribeck Curve when a number of link's velocities is related to a specific friction torque, as shown in the example in Fig. 3 with the main friction components. This curve summarizes all the friction data and is used as the primary means of completing the friction mathematical model. After defining how to monitor friction torque, links velocity and velocity profiles, the next step is the friction parameters acquisition.

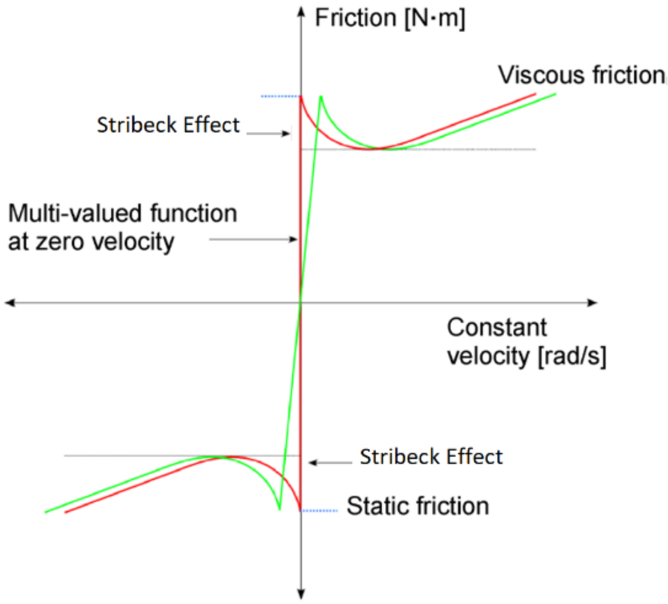

Fig. 3. Stribeck Curve and its friction component

2.3. Static Parameters

The identification of the four static parameters is a very established procedure due to two main factors, their linear behavior and the possibility of calculating them directly from the experimental data. The parameters F_C, F_S, $\dot{\theta}_S$ and σ_2 are found through the comparison between two Stribeck Curves, one created by the experimental data and the other by the numerical simulation using (8) to (10). The four values are found using the vector Xs in (13), the error $e_s(X_S, \dot{\theta}_m)$ in (14) and the cost function J_s to be minimized in (15).

$$X_s = [F_C, F_S, \dot{\theta}_S, \sigma_2] \tag{13}$$

$$e_s(X_S, \dot{\theta}_m) = \tau_f - \tau_f(X_S, \dot{\theta}_m) \tag{14}$$

$$J_S = \frac{1}{2}\sum_{i=1}^{n} e_s(X_S, \dot{\theta}_m)_i^2 \tag{15}$$

2.4. Dynamic Parameters

As previously mentioned, the experimental data acquisition to define the parameters σ_0 and σ_1 is done by adjusting the experimental setup so that it is possible to capture and highlight the data that are most influenced by these two parameters. In [43] and [54] describe σ_0 as the stiffness coefficient of the microscopic deformation of z during the Presliding displacement and σ_1 as the damping coefficient associated with the variation of the z deformation, dz/dt. Thus, the particularity in obtaining the dynamic parameters lies mainly in the fact that z is not a directly measurable parameter. A second complicating factor is commented on by [54], where it is not possible to use linear estimation methods directly in the experimental data as done for the static parameters due to the fact that there is a nonlinear relation between friction and the dynamic parameters. The stage called by [43] and [54] presiding displacement where σ_0 and σ_1 are evidenced it is described by [55] as the stage prior to movement where there is no visible joint displacement, but this visual absence does not indicate that the deformation has already started or that there are invisible deformations.

In [43], [55] point out that in the pre-sliding displacement, the bristles deformation can be considered $\theta \approx z$ during a certain period. The experimental setup is implemented to enhance the pre-sliding displacement by applying a ramp input on the actuator with a very slow increasing step so it is possible to acquire the position and torque data from the static state, the pre-sliding displacement and the break-away moment [55], [56].

The bristles deformation z can be estimated using (9) and ensuring that the system begins moving from absolute rest. The bristles deformation variation can be written as

$$\dot{z} = \omega - \frac{\tau_f}{F_S}|\omega| \tag{16}$$

The solution for the variable z can be done by integrating with (12) obtaining

$$z(t) = \theta(t) - \theta(0) + \frac{k_m k_c}{2F_S}\left(\theta(t)t + \int_0^t \theta(\tau)d\tau\right) \tag{17}$$

For an interval $(0, T)$ a set of n data of $z(t)$ and $\tau_f(t)$ are captured composing the vectors z and τ_f, respectively. In [55] and [57] shows that the initial value for σ_0 can be found by

$$\sigma_0 = \frac{Z^T \tau_f}{Z^T Z} \tag{18}$$

The value for σ_1 can be found by using the equation that describes the dynamic model for the actuator, in the case of this work, a DC motor as

$$J\ddot{\theta} = \tau - \tau_f \tag{19}$$

where J is the system inertia, τ is the input torque and τ_f is the friction torque and (8) of the friction model leading to

$$\tau = J\ddot{\theta} + \sigma_0\theta + (\sigma_1 + \sigma_2)\dot{\theta} \tag{20}$$

The solution of (20) can be made from the Laplace transform shown in (21), and the estimation is based on a second-order system obtained, as pointed out in (22).

$$\frac{\theta(S)}{\tau_f(S)} = \frac{1}{mS^2 + (\sigma_2 + \sigma_1)S + \sigma_0} \tag{21}$$

$$\sigma_1 = 2\xi m\sqrt{\frac{\sigma_0}{m}} - \sigma_2 \tag{22}$$

Although it is possible to find σ_0 and σ_1 using (18) and (22), there are situations where it is necessary to use the torque equation shown in (20) to estimate σ_0 and σ_1 together because the data obtained by the position sensors are not accurate enough to identify the Pre Sliding displacement. In such applications, the experimental torque data during the start of motion is used in a parameter identification method along with the torque in (16) to find σ_0 and σ_1. The results presented by [35] is an example of using the torque equation to calculate σ_0 and σ_1 directly and the results are proven effective by a Friction Compensation Control application.

In applications where position sensors allow sufficient accuracy [23] shows how to use the values for σ_0 and σ_1 from (18) and (22) as initial conditions can be done to find more accurate values for the dynamic parameters. In such cases, σ_0 and σ_1 from (18) and (22) are considered as initial conditions σ_0^0 and σ_1^0 for a parameter identification method using the torque (20) to minimize J_i shown in (23) using the Pre Sliding Displacement experimental data, a step very close to the method commenting on the approach with sensors without high precision commented above.

$$J_i = q_1 \sum_{i=1}^{n} (e_d(t))^2 + q_2\, max\{|e_d(t)|\} \tag{23}$$

where the error $e_d(t)$ is given by the difference between the experimental data θ_{ed} and the model simulation data θ_{md}, $e_d(t) = \theta_{ed}(t) - \theta_{md}(t)$, q_1 and q_2 are weight coefficients.

2.5. Experimental Setup

Fig. 4 shows the prototype of the robotic manipulator with the adaptation used to use only one of the links. Due to the structural characteristics of the motor used, the prototype structure is built in such a way that the sensor is positioned on the front of the actuator, where it is coupled to the link. In ideal situations, the sensing is done at the back of the actuator, leaving the frontal part without any restriction on the work volume allowing continuous rotation through 360°.

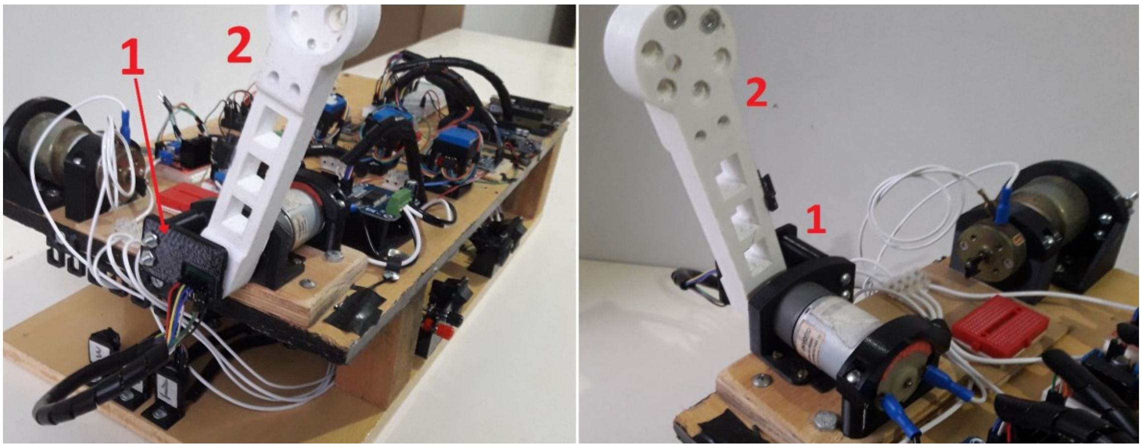

Fig. 4. Experimental setup for the first link of the robotic manipulator: Limitation imposed by the sensor support that prevents full rotation of the link: 1. Sensor Support, 2. Robot Link

The position data was taken using the AS5145H magnetic encoder from AMS. It is a 12 bits encoder with SSI communication with precision up to 0.008° composed of two parts, a magnet and an IC. A magnet is placed at the link, and the sensor IC measures the magnet's angular displacement through the Hall Effect, defining the link displacement.

The current i_j was taken using the LEM LA-25 NP current transducer and the ADC ADS1256, both linked with an Arduino Mega board. Fig. 4 shows the experimental setup using parts of the complete manipulator system shown in Fig. 1. The current transducer LEM 25-NP was used in the

5/1000 configuration, and a maximum of 800 mA current output resulting in a 670 Ω resistor at the output pin.

Fig. 5 shows the circuit used for current sensing. The actuator used was the AK555/11.1PF12R83CE-V2 from AKIMA. The DC motor works at a nominal voltage of 12 V, with a maximum velocity of 83 RPM and maximum torque of 11.1 kgf.cm. The link was designed specifically for this work using a 3D printer with PLA plastic polymer material with 21 cm of length, 5 cm of thickness, 4.5 cm of height and a total of 45 grams of weight.

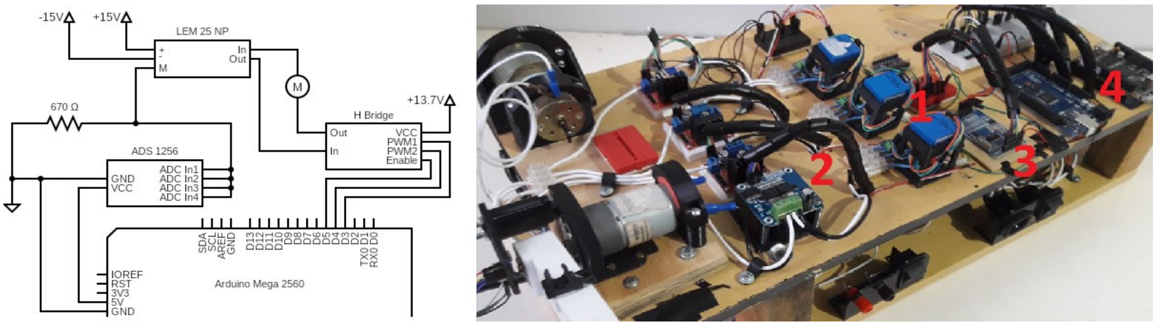

(a) (b)

Fig. 5. (a) Circuit for current measurement (b) 1. LEM LA-25 NP. 2. BTS 7680 H Bridge Driver, (3) ADC ADS1256, (4) Arduino Mega

All the sensors were read at 10 kHz from the controller, and the speed data were found with a 1 ms interruption from two consecutive position data. The PID controller used to find the Stribeck Velocity was used with the constants $K_p = 1.25$, $K_i = 3.15$, $K_d = 0.55$, and a sampling frequency of 1 kHz.

3. Results and Discussion

To obtain the six friction parameters, two experimental sessions were carried out, one for the four static parameters and another for the two dynamic ones. Considering the starting of the motor by PWM modulation via Arduino Mega, where a voltage ramp with a very slow increase gradually increases the voltage applied to the motor, allowing a soft start differentiating rest and axis movement. An AS5145H encoder is used to read the position of the motor shaft, and a moving average of 10 successive measurements is considered. For obtaining the static parameters is considered, the Stribeck Curve using experimental data of speed and torque collected in the robot link. Consider procedures similar to those proposed in [59], [60] and [61].

Due to the physical characteristics of the prototype used, the manipulator link does not allow free rotation, being possible to operate it only in a range of 30° to 310°. In this way, a PID control was used to control the speed in this range and close to the limits of 30° and 310° two deceleration stretches for a smooth reversal of rotational direction. The curve was constructed using twenty measurements of speed and torque with link operation counterclockwise, the direction adopted as positive velocity.

Fig. 6 shows the result of obtaining the static parameters through the App Curve Fitting of the MATLAB software using NonlinearLeastSquare as a method, True-Region algorithm and maximum error for 10^{-6}. The result of the estimated static parameters is $F_c = 2.002$, $F_c = 0.5843$, $\sigma_2 = 0.1328$ and $\dot{\theta} = 0.8379$.

Equations (14) and (18) directly to find σ_0 and σ_1 the values were found as $\sigma_0 = 1.937$ and $\sigma_1 = 1.401$. Using these values as the initial values for the dynamic parameter and the Non-linear Least Square curve fitting method with the pre-sliding data are obtained $\sigma_0 = 2.15$ and $\sigma_1 = 1.34$.

Comparison of experimental data with numerical data for the angular movement of the motor shaft can be seen in Fig. 7. Comparison of experimental data with numerical data for the Stribeck Curve can be seen in Fig. 8.

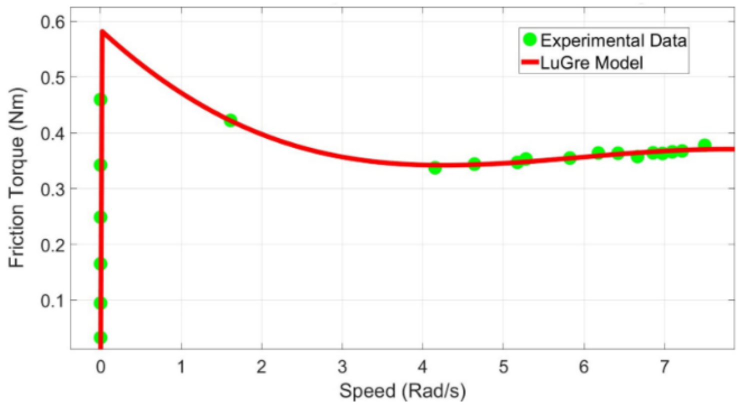

Fig. 6. Stribeck Curve: Curve Fitting using Experimental Data and the MATLAB App Curve Fitting

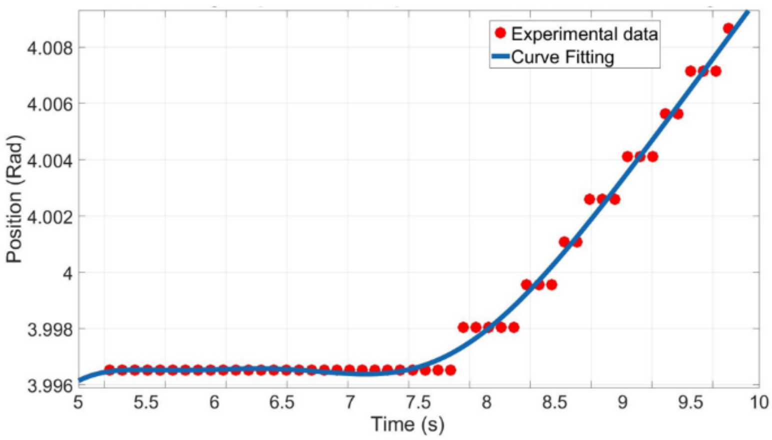

Fig. 7. Pre-Sliding displacement: Curve fitting using Experimental Data

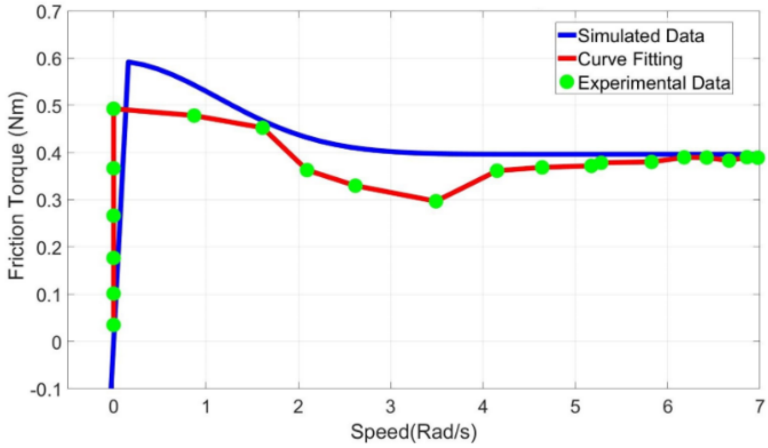

Fig. 8. Stribeck Curve: Comparison between experimental data and numerical simulation

Fig. 8 shows the friction torque variation for motor shaft speed variations, considering the experimental data and the numerical data obtained from the Lugre model. From the definition of the parameters, it is possible to complete the friction model shown in (8) to (10), obtain the simulation of the behavior of the friction of the robot's first link, and thus compare the numerical results with the experimental data, as shown in Fig. 7 and Fig. 8.

Another important point is the ability of the proposed mathematical model to represent the other phenomena observed in friction, such as Pre-Sliding displacement and Stick-Slip motion, shown in Fig. 9. As can be seen in the results presented, one of the most important contributions of the LuGre model is the capability to reproduce the robotic links to real physical phenomena during motion. To verify the model's effectiveness, a series of numerical simulations were made to reproduce the most important phenomena, the correct Stribeck Curve, as shown in Fig. 8.

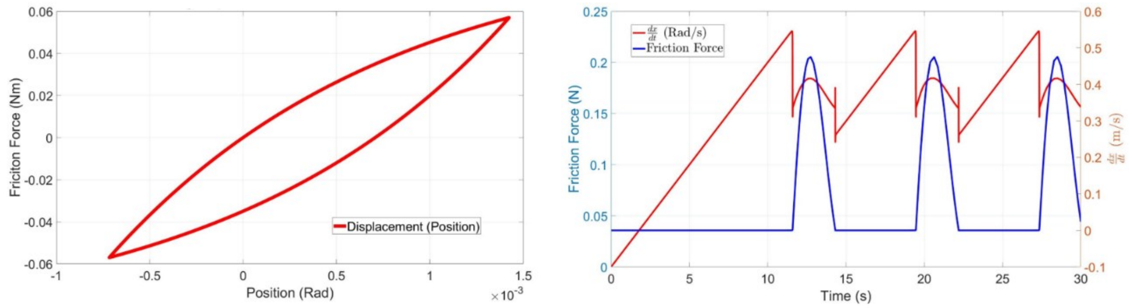

(a) (b)

Fig. 9. (a) Relation between friction force and position during the pre-sliding motion simulation (b) Stick-Slip motion for simulated data

4. Conclusion

This paper presents a friction model for a robotic manipulator with one degree of freedom using the LuGre model. The method to find the static and dynamic parameters was presented to complete the dynamic mathematical model for the robotic manipulator. The Virtual Torque Sensor presented by [58] used to estimate the link's torque was successful and used in conjunction with the matrix model to allow the friction torque data sensing without a specific force sensor. The MATLAB App Curve Fitting used to find the LuGre parameters presents an effective approximation and eliminates the need for a specific numerical algorithm design specifically for this purpose. The method shown by [43] and [55] was capable of finding the dynamic parameters $\sigma_0(Nms/rad)$ and $\sigma_1(Nms/rad)$, using the pre-sliding displacement data and the parameter identification process. As shown in Fig. 6 to Fig. 8, the friction model presented in this work is capable of representing the friction force for the robotic manipulator reproducing the main physical phenomena and can be used in future works involving the complete manipulator system shown in Fig. 1.

The data shown in Fig. 7 show that the maximum accuracy acquired in reading the position data during the Pre-sliding displacement was 0.002 rad, approximately 0.1145°, results similar to the results presented in [54] and [55], where a similar method was applied. The accuracy of the results obtained in this paper can be improved by combining data acquisition hardware with a high sampling rate and position sensors with greater precision than 14 bits.

Author Contribution: All authors contributed equally to the main contributor to this paper. All authors read and approved the final paper.

Funding: This research received no external funding.

Acknowledgment: The authors acknowledge the CAPES, FAPESP, FA and CNPq, both Brazilian research funding agencies.

Conflicts of Interest: The authors declare no conflict of interest.

References

[1] J. Kumar, V. Kumar, and K. P. S. Rana, "Fractional-order self-tuned fuzzy PID controller for three-link robotic manipulator system," *Neural Computing and Applications*, vol. 32, pp. 7235-7257, 2020, https://doi.org/10.1007/s00521-019-04215-8.

[2] M. Deng, S. Kubota, and Y. Xu, "Nonlinear Intelligent Control of Two Link Robot Arm by Considering Human Voluntary Components," *Sensors*, vol. 22, pp. 1-22, 2022, https://doi.org/10.3390/s22041424.

[3] P. Lu, W. Huang, J. Xiao, F. Zhou, and W. Hu, "Adaptive Proportional Integral Robust Control of an Uncertain Robotic Manipulator Based on Deep Deterministic Policy Gradient," *Mathematics*, vol. 9, pp. 1-16, 2021, https://doi.org/10.3390/math9172055.

[4] A. M. Tusset, J. J. De Lima, F. C. Janzen, P. L. Paula Filho, J. A. G. Luz Junior, J. M. Balthazar, and A. Kossoski, "Hybrid PID-LQR control applied in positioning control of robotic manipulators subject to excitation from non-ideal sources," *Mechanism and Machine Science, Springer*, vol. 116, pp. 393-403, 2022, https://doi.org/10.1007/978-3-030-96603-4_2.

[5] P. Mercorelli, "A Theoretical Dynamical Noninteracting Model for General Manipulation Systems Using Axiomatic Geometric Structures," *Axioms*, vol. 11, pp. 309, 2020, https://doi.org/10.3390/axioms11070309.

[6] C. Garriz and R. Domingo, "Development of trajectories through the Kalman algorithm and application to an industrial robot in the automotive industry," *IEEE Access*, vol. 7, pp. 23570-23578, 2019, https://doi.org/10.1109/ACCESS.2019.2899370.

[7] U. Zakia, M. Moallem, and C. Menon, "PID-SMC controller for a 2-DOF planar robot. 2019 International Conference on Electrical," *Computer and Communication Engineering (ECCE)*, pp. 1-5, 2019, https://doi.org/10.1109/ECACE.2019.8679436.

[8] B. Dong, T. An, F. Zhou, K. Liu, and Y. Li, "Decentralized robust zero-sum neuro-optimal control for modular robot manipulators in contact with uncertain environments: Theory and experimental verification," *Nonlinear Dyn.*, vol. 97, no. 1, pp. 503-524, 2019, https://doi.org/10.1007/s11071-019-04994-8.

[9] Z. Dachang, D. Baolin, Z. Puchen, and C. Shouyan, "Constant force PID control for robotic manipulator based on fuzzy neural network algorithm," *Complexity*, vol. 2020, pp. 1-11, 2020, https://doi.org/10.1155/2020/3491845.

[10] A. Carron, E. Arcari, M. Wermelinger, L. Hewing, M. Hutter, and M. N. Zeilinger, "Data-driven model predictive control for trajectory tracking with a robotic arm," *IEEE Robot. Autom. Lett.*, vol. 4, no. 4, pp. 3758-3765, 2019, https://doi.org/10.3929/ethz-b-000363021.

[11] Y. Mehmood, J. Aslam, N. Ullah, M. S. Chowdhury, K. Techato, and A. N. Alzaed, "Adaptive robust trajectory tracking control of multiple quad-rotor UAVs with parametric uncertainties and disturbances," *Sensors*, vol. 21, no. 7, pp. 2401, 2021, https://doi.org/10.3390/s21072401.

[12] N. Ullah, I. Sami, W. Shaoping, H. Mukhtar, X. Wang, M. S. Chowdhury, and K. Techato, "A computationally efficient adaptive robust control scheme for a quad-rotor transporting cable-suspended payloads," *J. Aerosp. Eng.*, pp. 1-17, 2021, https://doi.org/10.1177/09544100211013617.

[13] Y. Sun, J. Xu, H. Wu, G. Lin, and S. Mumtaz, "Deep learning based semi-supervised control for vertical security of maglev vehicle with guaranteed bounded airgap," *IEEE Trans. Intell. Transp. Syst.*, vol. 22, no. 7, pp. 4431-4442, 2021, https://doi.org/10.1109/TITS.2020.3045319.

[14] M. Van, X. P. Do, and M. Mavrovouniotis, "Self-tuning fuzzy PID-nonsingular fast terminal sliding mode control for robust fault tolerant control of robot manipulators," *ISA Transactions*, vol. 96, pp. 60-68, 2020, https://doi.org/10.1016/j.isatra.2019.06.017.

[15] S. A. Rad, M. G. Tamizi, A. Mirfakhar, M. T. Masouleh, and A. Kalhor, "Control of a two-DOF parallel robot with unknown parameters using a novel robust adaptive approach," *ISA Transactions*, vol.117, pp. 70-84, 2021, https://doi.org/10.1016/j.isatra.2021.02.001.

[16] S. Yang, J. Han, L. Xia, and Y-H Chen, "An optimal fuzzy-theoretic setting of adaptive robust control design for a lower limb exoskeleton robot system," *Mechanical Systems and Signal Processing*, vol. 141, pp. 106706, 2020, https://doi.org/10.1016/j.ymssp.2020.106706.

[17] E-H. Guechi, S. Bouzoualegh, Y. Zennir, S. Blažiˇc, and "MPC Control and LQ Optimal Control of A Two-Link Robot Arm: A Comparative Study," *Machines*, vol. 6, pp. 409-414, 2018, https://doi.org/10.3390/machines6030037.

[18] M. H. Korayem, M. Irani, and S. R. Nekoo, "Load maximization of flexible joint mechanical manipulator using nonlinear optimal controller," *Acta Astronautica*, vol. 69, pp. 458-469, 2011, https://doi.org/10.3390/machines6030037.

[19] M. H. Korayem, M. Irani, and S. R. Nekoo, "Analysis of manipulators using SDRE: a closed loop nonlinear optimal control approach," *Scientia Iranica. Transaction B, Mechanical Engineering*, vol. 17, pp. 456-467, 2010, http://scientiairanica.sharif.edu/article_3368.html.

[20] M. H. Korayem and S. R. Nekoo, "Finite-time state-dependent Riccati equation for time-varying nonaffine systems: rigid and flexible joint manipulator control," *ISA Transactions*, vol. 54, pp. 125–144, 2015, https://doi.org/10.1016/j.isatra.2014.06.006.

[21] M. H. Korayem and S. R. Nekoo, "State-dependent differential Riccati equation to track control of time-varying systems with state and control nonlinearities," *ISA Transactions*, vol. 57, pp. 117–135, 2015, https://doi.org/10.1016/j.isatra.2015.02.008.

[22] J. J. Lima, A. M. Tusset, F. C. Janzen, V. Piccirillo, C. B. Nascimento, J. M. Balthazar, and M. R. L. F. Brasil, "SDRE applied to position and vibration control of a robot manipulator with a flexible link," *Journal of Theoretical and Applied Mechanics*, vol. 54, pp. 1067–1078, 2016, https://doi.org/10.1016/j.isatra.2015.02.008.

[23] J. J. Lima, J. M. Balthazar, R. T. Rocha, F. C. Janzen, D. Bernardini, G. Litak, A. M. Tusset, and D. Bassinello, "On Positioning and Vibration Control Application to Robotic Manipulators with a Nonideal Load Carrying," *Shock and Vibration*, vol. 2019, pp. 5408519, 2019, https://doi.org/10.1155/2019/5408519.

[24] A. M. Tusset, J. J. De Lima, F. C. Janzen, P. L. Paula Filho, J. A. G. Luz Junior, J. M. Balthazar, and A. Kossoski, "A Hybrid PID-LQR Control Applied in Positioning Control of Robotic Manipulators Subject to Excitation from Non-ideal Sources," *Mechanisms and Machine Science*, pp. 393-403, 2022, https://doi.org/10.1007/978-3-030-96603-4_21.

[25] A. M. Tusset, A. E. B. Pereira, J. M. Balthazar, F. C. Janzen, C. Oliveira, M. E. K. Fuziki, and G. G. Lenzi, "Positioning Control of Robotic Manipulators Subject to Excitation from Non-Ideal Sources," *Robotics*, vol. 12, pp. 51, 2023, https://doi.org/10.3390/robotics12020051.

[26] O. Saleem, F. Abbas, and J. Iqbal, "Complex Fractional-Order LQIR for Inverted-Pendulum-Type Robotic Mechanisms: Design and Experimental Validation," *Mathematics*, vol. 11, pp. 913, 2023, https://doi.org/10.3390/math11040913.

[27] K. Ali, A. Mehmood, I. Muhammad, S. Razzaq, and J. Iqbal, "Control of an Anthropomorphic Manipulator using LuGre Friction Model-Design and Experimental Validation," *Journal of Mechanical Engineering*, vol. 67, pp. 401-410, 2021, https://doi.org/10.5545/sv-jme.2021.7258.

[28] K. Ali, S. Ullah, A. Mehmood, H. Mostafa, M. Marey, and J. Iqbal, "Adaptive FIT-SMC Approach for an Anthropomorphic Manipulator with Robust Exact Differentiator and Neural Network-Based Friction Compensation," *IEEE Access*, vol. 10, pp. 3378-3389, 2022, https://doi.org/10.1109/ACCESS.2021.3139041.

[29] A. Asghar, M. Iqbal, A. Khaliq, S. Rehman, and J. Iqbal, "Performance comparison of structured H∞ based looptune and LQR for a 4-DOF robotic manipulator," *PLOS ONE*, 2022, vol. 17, no. 4, pp. e0266728, 2022, https://doi.org/10.1371/journal.pone.0266728.

[30] A. Rezoug, J. Iqbal, M. Tadjine, "Extended grey wolf optimization–based adaptive fast nonsingular terminal sliding mode control of a robotic manipulator," *Proceedings of the Institution of Mechanical Engineers, Part I: Journal of Systems and Control Engineering*, vol. 236, pp. 1738-1754, 2022, https://doi.org/10.1177/09596518221099768.

[31] S. Ullah, A. Mehmood, Q. Khan, S. Rehman, and J. Iqbal, "Robust integral sliding mode control design for stability enhancement of under-actuated quadcopter," *Int. J. Control, Autom. Syst.*, vol. 18, no. 7, pp. 1671-1678, 2020, https://doi.org/10.1007/s12555-019-0302-3.

[32] J. Hu, Y. Wang, L. Liu, and Z. Xie, "High-accuracy robust adaptive motion control of a torque-controlled motor servo system with friction compensation based on neural network," *Proc. Inst. Mech. Eng, C, J. Mech. Eng. Sci.*, vol. 233, no. 7, pp. 2318-2328, 2019, https://doi.org/10.1177/09544062187830.

[33] B. Denkena, B. Bergmann, and D. Stoppel, "Reconstruction of process forces in a five-axis milling center with a LSTM neural network in comparison to a model-based approach," *J. Manuf. Mater. Process.*, vol. 4, no. 3, pp. 62, 2020, https://doi.org/10.3390/jmmp4030062.

[34] S.-H. Han, M. S. Tran, and D.-T. Tran, "Adaptive sliding mode control for a robotic manipulator with unknown friction and unknown control direction," *Appl. Sci.*, vol. 11, no. 9, pp. 3919, 2021, https://doi.org/10.3390/app11093919.

[35] Z. Zhou and B.Wu, "Adaptive sliding mode control of manipulators based on fuzzy random vector function links for friction compensation," *Optik*, vol. 227, pp. 166055, 2021, https://doi.org/10.1016/j.ijleo.2020.166055.

[36] L. Zhang, J. Wang, J. Chen, K. Chen, B. Lin, and F. Xu, "Dynamic modeling for a 6-DOF robot manipulator based on a centrosymmetric static friction model and whale genetic optimization algorithm," *Adv. Eng. Softw.*, vol. 135, pp. 102684, 2019, https://doi.org/10.1016/j.advengsoft.2019.05.006.

[37] A. Khurram, A. Mehmood, I. Muhammad, S. Razzaq, and J. Iqbal, "Control of an Anthropomorphic Manipulator using LuGre Friction Model - Design and Experimental Validation," *Journal of Mechanical Engineering*, vol. 67, pp. 401-410, 2021, https://doi.org/10.5545/sv-jme.2021.7258.

[38] K. Ali, S. Ullah, A. Mehmood, H. Mostafa, M. Marey, and J. Iqbal, "Adaptive FIT-SMC Approach for an Anthropomorphic Manipulator with Robust Exact Differentiator and Neural Network-Based Friction Compensation," *IEEE Access*, vol. 10, pp. 3378-3389, 2022, https://doi.org/10.1109/ACCESS.2021.3139041.

[39] X. Tu, Y. Zhou, P. Zhao, and X. Cheng, "Modeling the Static Friction in a Robot Joint by Genetically Optimized BP Neural Network," *J. Intell. Robot. Syst*, vol. 94, pp. 29–41, 2019, https://doi.org/10.1007/s10846-018-0796-6.

[40] A. C. Bitterncourt, E. Wernholt, S. Sander-Tavallaey, and T. Brogardh, "An Extended Friction Model to Capture Load and Temperature Effects in Robot Joints," *IEEE Int. Conf. Intell. Robots Syst*, pp. 6161-6167, 2010, https://doi.org/10.1109/IROS.2010.5650358.

[41] Y. Zhang, "Design and Synthesis of Mechanical systems with Coupled Units," *Mechanical Engineering*, Rennes, 2019, https://theses.hal.science/tel-02307221/document.

[42] D. R. Dentler, "Design, Control and Implementation of a Three Link Articulated Robot Arm," *Thesis,* Faculty of The University of Akron, 2008, https://etd.ohiolink.edu/apexprod/rws_olink/r/1501/10?clear=10&p10_accession_num=akron1217208877.

[43] C. C.-De-Wit and P. Lischinsky, "Adaptive Friction Compensation with Partially Know Dynamic Friction Model," *Int J Adapt Control Signal Process*, vol. 11, pp. 65-80, 1997, https://doi.org/10.1002/(SICI)1099-1115(199702)11:1%3C65::AID-ACS395%3E3.0.CO;2-3.

[44] B. Li, Y. Zhang, L. Yuan, and X. Xi, "Study on the Low Velocity Stability of a Prostate Seed Implantation Robot's Rotatory Joint," *Electronics*, vol. 9, pp. 284, 2020, https://doi.org/10.3390/electronics9020284.

[45] J. L. P. Felix, J. M. Balthazar, R. M. Brasil, and B. R. Pontes Jr, "On lugre friction model to mitigate nonideal vibrations," *J. Comput. Nonlinear Dyn*, vol. 4, pp. 034503, 2009, https://doi.org/10.1115/1.3124783.

[46] V. Piccirillo, A. M. Tusset, and J. M. Balthazar, "Chaos control and impact suppression in rotor-bearing system using magnetorheological fluid," *The European Physical Journal. Special Topics*, vol. 224, pp. 3023-3040, 2015, https://doi.org/10.1140/epjst/e2015-02604-7.

[47] A. M. Tusset, V. Piccirillo, J. M. Balthazar, and M. R. L. F. Brasil, “On suppression of chaotic motions of a portal frame structure under non-ideal loading using a magneto-rheological damper,” *Journal of Theoretical and Applied Mechanics (Warsaw),* vol. 53, pp. 653-664, 2015, https://doi.org/10.15632/jtam-pl.53.3.653.

[48] L. Simoni, M. Beschi, A. Visioli, and K. J. Åström, “Inclusion of the dwell time effect in the LuGre friction model,” *Mechatronics*, vol. 66, pp. 102345, 2020, https://doi.org/10.1016/j.mechatronics.2020.102345.

[49] A. Tusset, F. Janzen, V. Piccirillo, R. T. Rocha, J. M. Balthazar, and G. Litak, “On nonlinear dynamics of a parametrically excited pendulum using both active control and passive rotational (MR) damper,” *Journal of Vibration and Control*, vol. 24, pp. 1587-1599, 2018, https://doi.org/10.1177/1077546317714882.

[50] D. A. Haessig and B. Friedland, “On the Modeling and Simulation of Friction,” *J Dyn Syst Meas Control*, vol. 114, pp. 354-362, 1991, https://doi.org/10.1115/1.2896418.

[51] Q. Chen, L. Tao, Y. Nan, and X. Ren, “Adaptative Nonlinear Sliding Mode Control of Mechanical Servo System with LuGre Friction Compensation,” *J. Comput. Nonlinear Dyn. Control*, vol. 138, no. 138, pp. 021003, 2016, https://doi.org/10.1115/1.4032068.

[52] L. Gao, J. Yan, Z. Han, S. Wang, and N. Wang, “A Friction Model with Velocity, Temperature and Load Torque Effects for Collaborative Industrial Robot Joint,” *IEEE Int. Conf. Intell. Robots Syst.*, pp. 24-27, 2017, https://doi.org/10.1109/IROS.2017.8206141.

[53] M. R. Kermani, R. V. Patel, and M. Moallem, “Friction Identification and Compensation in Robot Manipulators,” *IEEE Trans. Instrum. Meas*, vol. 6, pp. 56-68, 2007, https://doi.org/10.1109/TIM.2007.907957.

[54] P. Lischinsky, C. Canudas-de-Wit, and G. Morel, “Friction Compensation for an Industrial Hydraulic Robot,” *IEEE Control Systems*, vol. 19, pp. 25-32, 1999, https://doi.org/10.1109/37.745763.

[55] X. Wang, S. Lin, and S. Wang, “Dynamic Friction Parameter Identification Method with LuGre Model for Direct-Drive Rotary Torque Motor,” *Math. Prob. Eng.,* vol. 2016, pp. 6929457, 2016, https://doi.org/10.1155/2016/6929457.

[56] J. Piasek, R. Patelski, D. Pazderski, and K. Krzyszrof, “Identification of a Dynamic Friction Model and its Application in a Precise Tracking Control,” *ACTA Polytech Hung*, vol 16, pp. 93-99, 2019, https://doi.org/10.12700/APH.16.10.2019.10.6.

[57] Y. Sun, T. Chen, and C. Shafai, “Parameter Identification of LuGre Friction Model: Experimental Set-up Design and Measurement,” *Int Mech. Eng. Congress. Expo.,* vol 11, pp. 1319, 2015, https://doi.org/10.1115/IMECE2015-51255.

[58] L. Simoni, E. Villagrossi, M. Beschi, A. Marini, N. Pedrocchi, L. M. Tosatti, G. Legnani, and A. Visioli, “On the use of a temperature based friction model for a virtual force sensor in industrial robot manipulators,” *22nd IEEE International Conference on Emerging Technologies and Factory Automation (ETFA)*, pp. 1-6, 2017, https://doi.org/10.1109/ETFA.2017.8247655.

[59] F. C. Janzen, “Position and Vibration Control of a Flexible Structure in Slewing Motion by Applying Shape Memory Alloys,” *Dissertation, Mechanical Engineering, Sao Paulo State University*, 2016, https://repositorio.unesp.br/handle/11449/144649.

[60] S. Nithya B., Mythile A., Pavithra S., and Nivetha N., “Parameter Identification of a DC Motor,” *International Journal of Science & Technology Research*, vol. 9, no. 2, 2020, http://www.ijstr.org/final-print/feb2020/Parameter-Identification-Of-A-Dc-Motor.pdf.

[61] W. S. Chaves, E. H. Kaneko, M. F. Mollon, L. Niro, A. N. Vargas, and M. A. F. Montezuma, “Parameters Identification of a Direct Current Motor Using the Trust Region Algorithm,” *International Journal of Advanced Engineering Research and Science*, vol. 4, no. 12, 2017, https://doi.org/10.22161/ijaers.4.12.24.